

## A LIKELY REDBACK MILLISECOND PULSAR COUNTERPART OF 3FGL J0838.8–2829

J. P. HALPERN<sup>1</sup>, J. STRADER<sup>2</sup>, AND M. LI<sup>1</sup>  
(Received 2017 June 14; Accepted 2017 June 28)

## ABSTRACT

We obtained new optical observations of the X-ray source XMMU J083850.38–282756.8, the previously proposed counterpart of the  $\gamma$ -ray source 3FGL J0838.8–2829. Time-series photometry in the  $r'$  band reveals periodic modulation of  $\approx 1$  magnitude that is characteristic of the heating of the photosphere of a low-mass companion star by a compact object. The measured orbital period is  $5.14817 \pm 0.00012$  hr. The shape of the light curve is variable, evidently due to the effects of flaring and asymmetric heating. Spectroscopy reveals a companion of type M1 or later, having a radial velocity amplitude of  $315 \pm 17$  km s<sup>-1</sup>, with period and phasing consistent with the heating interpretation. The mass function of the compact object is  $0.69 \pm 0.11 M_{\odot}$ , which allows a neutron star in a high-inclination orbit. Variable, broad H $\alpha$  emission is seen, which is probably associated with a wind from the companion. These properties, as well as the X-ray and  $\gamma$ -ray luminosities at the inferred distance of  $< 1.7$  kpc, are consistent with a reback millisecond pulsar in its non-accreting state. A search for radio pulsations is needed to confirm this interpretation and derive complete system parameters for modeling, although absorption by the ionized wind could hinder such detection.

*Subject headings:* gamma rays: stars — pulsars: general — X-rays: individual (XMMU J083850.38–282756.8)

## 1. INTRODUCTION

A major achievement of the Large Area Telescope on the *Fermi* Gamma-ray Observatory is the detection of many recycled millisecond pulsars (MSPs), some of which are accomplished with the help of prior radio ephemerides, but most of them are new ones that are found in successful radio-pulsar searches of its unidentified  $\gamma$ -ray source error circles. Of the 205 pulsars detected by *Fermi* so far, 92 are recycled<sup>3</sup>. Most interesting among the *Fermi* MSP discoveries are the black widow (BW) and “reback” binary systems (Roberts 2013). BWs have companions of substellar mass, while rebacks have  $> 0.1 M_{\odot}$ , bloated companions that are usually close to filling their Roche lobes. Both BWs and rebacks are compact binaries, with orbital periods  $\lesssim 1$  day. Their properties connect BWs and rebacks to their long-supposed low-mass X-ray binary (LMXB) progenitors, which spin them up by accretion (Alpar et al. 1982). A direct link was forged by the three rebacks that have been observed to transition between radio pulsar and accreting states on timescales of years: PSR J1023+0038 (Archibald et al. 2009), XSS J12270–4859 (Bassa et al. 2014; Roy et al. 2015), and PSR J1824–2452I in the globular cluster M28 (Papitto et al. 2013). Currently,  $\approx 60$  BW and reback pulsars are known that are almost equally divided between globular clusters and Galactic field populations<sup>4</sup>.

In addition to the BW and reback systems that are

certified radio MSPs, it has become possible through X-ray and optical follow-up of *Fermi* source error circles to identify counterparts that are almost certainly MSP binaries, even without obtaining a radio-pulsar detection. Their distinctive optical and X-ray light curves, spectroscopic orbital parameters, and positional coincidence with a  $\gamma$ -ray source allow some objects to be classified as BW or reback pulsars whose spin parameters are not yet known. *Fermi* sources that have been identified in this way are 3FGL J0212.1+5320 (Li et al. 2016; Linares et al. 2017), 1FGL J0523.5–2529 (Strader et al. 2014), 2FGL J1311.7–3429 (Kataoka et al. 2012; Romani 2012; Romani et al. 2012, 2015), 2FGL J1653.6–0159 (Kong et al. 2014; Romani et al. 2014), 3FGL J2039.6–5618 (Romani 2015; Salvetti et al. 2015), and 1FGL J2339.7–0531 (Romani & Shaw 2011; Kong et al. 2012). Radio pulsations at 2.88 ms were subsequently detected from 1FGL J2339.7–0531/PSR J2339–0533 by Ray et al. (2014), and 2.56 ms pulsations were found in  $\gamma$ -rays from 2FGL J1311.7–342/PSR J1311–3430 (Pletsch et al. 2012) with the help of its optical orbital ephemeris.

Complementing the above list of sources, 3FGL J0427.9–6704 (Strader et al. 2016), and 3FGL J1544.6–1125 (Bogdanov & Halpern 2015) have X-ray/optical counterparts that appear to be transitional MSPs in the accreting state. A related discovery is 3FGL J1417.5–4402/PSR J1417–4402, with a giant companion in a 5.4 day orbit (Strader et al. 2015) and 2.66 ms radio pulsations (Camilo et al. 2016). It is thought to be a typical MSP observed in the late stages of recycling, one that will end its evolution with a white dwarf companion in a several day orbit. The difficulty of detecting radio pulsations over most of the orbit of PSR J1417–4402, as well as from most rebacks, is apparently due to the absorption by the winds from their companions. This suggests that some  $\gamma$ -ray pulsars may be completely enshrouded most of the time (as proposed

<sup>1</sup> Columbia Astrophysics Laboratory, Columbia University, 550 West 120th Street, New York, NY 10027-6601, USA; jules@astro.columbia.edu

<sup>2</sup> Center for Data Intensive and Time Domain Astronomy, Department of Physics and Astronomy, Michigan State University, East Lansing, MI 48824, USA

<sup>3</sup> <https://confluence.slac.stanford.edu/display/GLAMCOG/Public+List+of+LAT-Detected+Gamma-Ray+Pulsars>

<sup>4</sup> <https://apatruno.wordpress.com/about/millisecond-pulsar-catalogue/>

TABLE 1  
LOG OF TIME-SERIES PHOTOMETRY<sup>a</sup>

Telescope/Instrument	Date (UTC)	Time (UTC)
MDM 2.4 m/OSMOS	2016 Dec 24	07:27–12:29
MDM 2.4 m/OSMOS	2016 Dec 27	07:02–12:41
LCO 1 m/Sinistro	2017 Jan 2	02:00–07:56
MDM 2.4 m/OSMOS	2017 Jan 28	05:01–09:57
MDM 2.4 m/OSMOS	2017 Feb 25	02:57–08:20
LCO 1 m/Sinistro	2017 Mar 27–28	23:27–05:33

<sup>a</sup> All exposures are 300 s in the  $r'$  filter.

by Tavani 1991) and will remain as only putative MSPs unless their pulsations can be found in X-rays or  $\gamma$ -rays.

Several authors have performed systematic analyses of the spectral and temporal properties of unidentified *Fermi* sources using machine learning techniques to assign the tentative classifications as active galactic nuclei, young pulsars, or MSPs (Ackermann et al. 2012; Lee et al. 2012; Mirabal et al. 2012, 2016; Saz Parkinson et al. 2016). In particular, Mirabal et al. (2016) classified 3FGL J0838.8–2829 among the high-confidence MSPs. In Halpern et al. (2017, Paper I), we identified a candidate binary MSP counterpart for 3FGL J0838.8–2829 from an *XMM-Newton* X-ray and optical study of its error circle (see also Rea et al. 2017), as well as in our own ground-based optical data. In this paper, we report on new optical and radio observations that characterize the source, XMMU J083850.38–282756.8. Section 2 describes time-series photometry that determines its 5.15 hr orbital period and characterizes the orbital light curve. Section 3 reports spectroscopy that yields a radial velocity curve for the secondary, and reveals variable, broad H $\alpha$  emission lines. Section 4 presents tentative inferences about the binary parameters, distance, and luminosity, and discusses the heating light curve and flaring activity and possible interpretations of the H $\alpha$  emission line. Section 5 summarizes the main conclusions.

## 2. TIME-SERIES PHOTOMETRY

Over 3 months in 2016–2017 we obtained six nights of time-series photometry of XMMU J083850.38–282756.8, the MSP candidate for 3FGL J0838.8–2829 from Paper I and Rea et al. (2017) using either the MDM Observatory 2.4m Hiltner telescope and Ohio State Multi-Object Spectrograph (OSMOS; Martini et al. 2011) in imaging mode, or a robotic 1m telescope at the CTIO node of the Las Cumbres Observatory (LCO) with its Sinistro imager (Brown et al. 2013). A log of the observations is given in Table 1. An SDSS  $r'$  filter was used in each case with an exposure time of 300 s. Run lengths ranged between 5 and 6 hours. The goals of this single-filter observing program were to obtain a precise orbital ephemeris, to monitor for rapid flaring as was seen in one of the *XMM-Newton* observations (Paper I), and to characterize any other variability of the light curve.

The optical position listed in Table 2 was derived from a 2.4m image using stars from the USNO B1.0 catalog (Monet et al. 2003) for an astrometric solution, and is consistent with the optical position given in Paper I. The 0''.3 error indicated in each coordinate includes the nominal uncertainty of the catalog coordinates.

Differential photometry and magnitude calibration

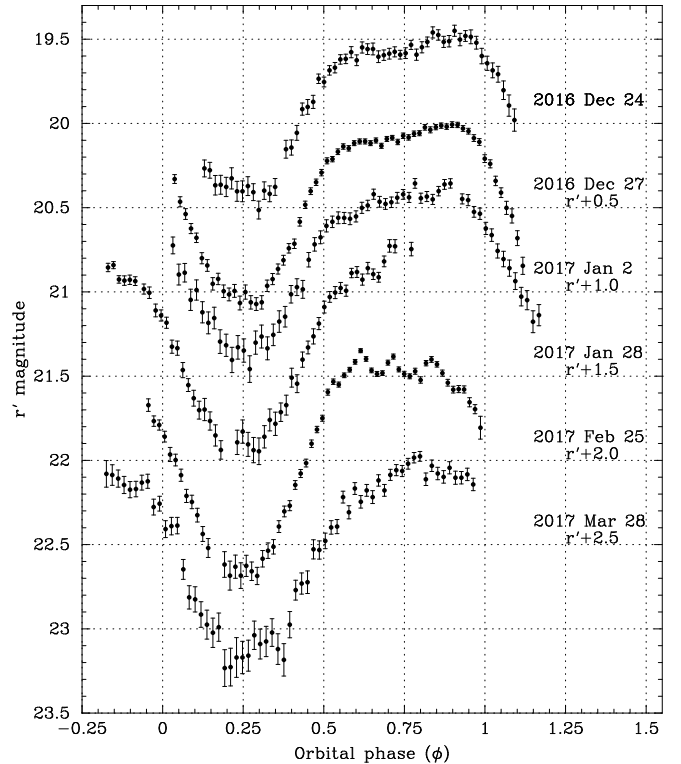


FIG. 1.— Optical light curves as a function of orbital phase according to the ephemeris in Table 2. A log of the observations is given in Table 1. Each data set after 2016 December 24 is displaced downward by a multiple of 0.5 mag for clarity.

were performed with respect to a calibrated comparison star. Images were inspected for cosmic-ray contamination, and a few points were rejected for cosmic-ray hits. The six resulting light curves are shown in Figure 1 as a function of orbital phase, the determination of which is described below. Here we adopt the convention in which phase zero is the ascending node of the pulsar,  $\phi = 0.25$  is the inferior conjunction of the companion, and  $\phi = 0.75$  is the superior conjunction. The shape of the light curve is characteristic of the heating of the side of the companion facing the pulsar, with a maximum brightness of  $r' \approx 19.5$  and a minimum of  $r' \approx 20.6$ .

There is occasional flaring, which is most easily visible in the 2017 January 28 and February 25 light curves in Figure 1. A quiescent state, if one can be recognized in the data, is perhaps best represented by the smooth light curve on 2016 December 27. It shows a sloping maximum that is not symmetric about the expected phase 0.75 of peak heating, but is rising up to  $\phi = 0.90$ . Such behavior is not uncommon among redbacks (Woudt et al. 2004; Li et al. 2014; Deneva et al. 2016), indicating that the heating of the companion is frequently not symmetric about the line connecting the stars.

In order to derive an orbital ephemeris in the presence of flaring and other possible sources of variable asymmetry of the light curve, we use the epoch of minimum in the light curve as  $\phi = 0.25$ , the fiducial phase, presuming that the timing of the minimum would be least affected by variability. Mid-times of each exposure were converted to barycentric dynamical time (TDB) using the utility of Eastman et al. (2010). Approximately 25 points around each minimum were fitted to a quadratic,

TABLE 2  
PHOTOMETRIC ORBITAL EPHEMERIS

Parameter	Value
R.A. (J2000)	08 <sup>h</sup> 38 <sup>m</sup> 50 <sup>s</sup> .44(2)
Decl. (J2000)	−28°27′57″.3(3)
Time span (MJD)	57746–57840
Epoch $T_0$ (MJD TDB) <sup>a</sup>	57781.2524(8)
Orbital period $P_{\text{orb}}$ (day)	0.214507(5)

<sup>a</sup> Epoch of the ascending node of the putative pulsar  $\phi = 0$  in Figure 1.

and the calculated epochs of minimum were fitted to a constant orbital period,  $P_{\text{orb}} = 5.14817 \pm 0.000012$  hr. The precise parameter values are listed in Table 2, with the epoch of pulsar ascending node  $T_0$  taken to be at  $\phi = 0$ . The average residual of the epochs of minimum from the fitted ephemeris is  $\approx 2$  minutes. For the ephemeris presented here we did not use the first observation (2016 December 24) as its minimum was poorly determined due to bad seeing, although its inclusion does not change the results within their errors.

### 3. OPTICAL SPECTROSCOPY

We performed spectroscopy on four different nights, from 2017 February 3 to April 24 (UT), with the Goodman spectrograph (Clemens et al. 2004) on the Southern Astrophysical Research (SOAR) telescope. On the first night spectra were taken with a 1200 l mm<sup>−1</sup> grating and a 1.''03 wide slit over the wavelength range of 7700–8700 Å, yielding a resolution of 1.6 Å. The remaining observations all used a 400 l mm<sup>−1</sup> grating and a 1.''03 slit over the wavelength range 4800–8830 Å, giving a resolution of 5.4 Å. The exposure times ranged from 900 to 1500 s, depending on the brightness of the source and the seeing. The spectra were reduced in the standard manner. Molecular bands indicate that the companion star is a late K or early M type, probably M0–M1 on the night side, and slightly hotter on the illuminated side.

We derived barycentric radial velocities through cross-correlation with bright stars taken with the same setup. Generally we used the region of the Ca II near-infrared triplet, but we substituted the region around Mg*b* for spectra with low signal-to-noise in the Ca II triplet region. The respective epochs for each spectrum are given as Modified Julian Day (MJD) in the TDB system. Given the faintness of the star, the formal radial velocity uncertainties are themselves uncertain, but the final results are nevertheless robust (see below). The radial velocity data are listed in Table 3.

Since the orbital period and time of ascending node are determined with more precision from the photometry than is possible from the presently limited spectroscopy, we adopted the photometric values of  $P_{\text{orb}}$  and  $T_0$  from Table 2, nonetheless finding that the photometric values fall within the uncertainties resulting from an independent fit to the radial velocities only. Given the short period and presumed long history of the system, we also assume zero eccentricity. Hence, the only free parameters are the velocity semi-amplitude of the secondary  $K_2$  and the systemic velocity  $v_{\text{sys}}$ . Using a circular Keplerian fit, we find best-fit values of  $K_2 = 315 \pm 17$  km s<sup>−1</sup> and  $v_{\text{sys}} = 129 \pm 15$  km s<sup>−1</sup>, with the uncertainties de-

TABLE 3  
BARYCENTRIC RADIAL VELOCITIES

UT Date	MJD (TDB)	Exposure (s)	$v_r$ (km s <sup>−1</sup> )	$\sigma(v_r)$ (km s <sup>−1</sup> )
2017 Feb 3	57787.1650	900	342.3	25.6
2017 Feb 3	57787.1756	900	316.8	25.0
2017 Feb 12	57796.1260	1200	339.2	25.5
2017 Feb 12	57796.1444	1200	465.9	22.5
2017 Mar 28	57840.1192	1200	436.0	28.3
2017 Mar 28	57840.1332	1200	431.3	37.7
2017 Mar 28	57840.1513	1200	407.9	27.1
2017 Mar 28	57840.1653	1200	377.1	32.4
2017 Mar 28	57840.1839	1200	125.4	25.7
2017 Apr 24	57867.0436	1200	−222.4	21.2
2017 Apr 24	57867.0576	1200	−184.7	23.5
2017 Apr 24	57867.0756	1200	−117.3	24.0
2017 Apr 24	57867.0896	1200	20.2	21.6
2017 Apr 24	57867.1269	1500	289.0	20.5

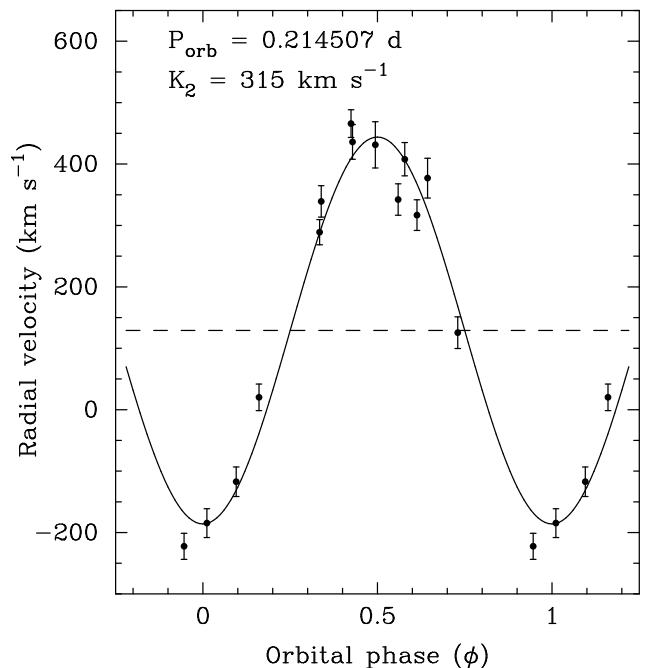


FIG. 2.— Spectroscopic radial velocities from Table 3 and best-fit sinusoid assuming the photometric orbital ephemeris of Table 2. The systemic velocity (dashed line) is  $v_{\text{sys}} = 129 \pm 15$  km s<sup>−1</sup>.

termined via bootstrap. This immediately yields a mass function of  $0.69 \pm 0.11 M_{\odot}$  for the compact object. If we instead assume that all radial velocities have the same uncertainties, the best-fit  $K_2$  and  $v_{\text{sys}}$  do not change. The best-fit radial velocity curve is shown in Figure 2.

In addition to the radial velocities, a notable feature of the optical spectra is the variable Balmer-line emission. The spectra on 2017 February 12 show remarkably broad, asymmetric H $\alpha$  emission (this is the only night where H $\beta$  emission, which is similarly broad, is clearly present). On 2017 March 28 the H $\alpha$  emission is present, but weak. In the last set of data, from 2017 April 24, the emission is stronger, though still not as strong as on 2017 February 12. Figure 3 shows the H $\alpha$  emission lines on the days when it was strongest. The maximum observed equivalent width was  $\approx 90$  Å. The FWHM ranges from 550–1510 km s<sup>−1</sup>, accounting for the spectral resolution. The line is generally asymmetric and sometimes double-

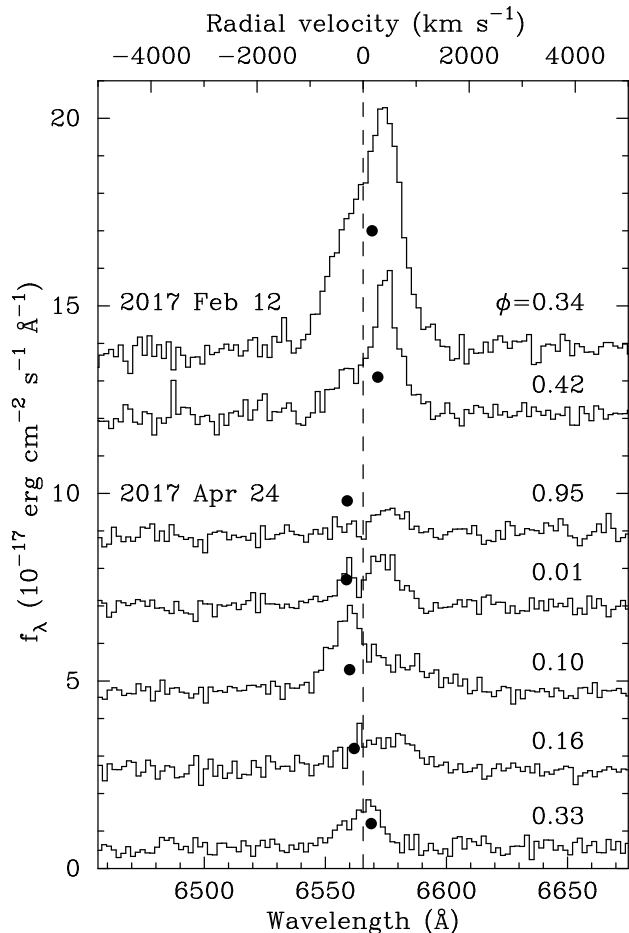


FIG. 3.— Selected spectra, two from 2017 February 12 and five from 2017 April 24, showing a broad  $H\alpha$  emission line. Spectra have been shifted upward in steps of  $2 \times 10^{-17} \text{ erg cm}^{-2} \text{ s}^{-1} \text{ \AA}^{-1}$  for clarity. The vertical dashed line represents the wavelength of  $H\alpha$  at the systemic velocity of the binary. The binary orbital phase according to the ephemeris of Table 2 is labeled. The filled circles indicate for each spectrum the fitted radial velocity of the companion relative to the center-of-mass (systemic) velocity.

peaked, with peak separations of  $520\text{--}770 \text{ km s}^{-1}$ . It is difficult to trace the velocities of the emission line due to the changing strengths of its multiple components. While they are shifted from the absorption-line radial velocities, there is no clear pattern with respect to orbital phase. However, there is often a peak in the line at or near the radial velocity of the companion, as marked in Figure 3.

## 4. DISCUSSION

### 4.1. Binary Parameters, Distance, and Luminosity

Assuming that the intrinsic spectral type of the companion star is M1 or later (because some of the heated side may still be visible at minimum light), its mass and radius are  $< 0.53 M_{\odot}$  and  $< 0.49 R_{\odot}$ , respectively (Pecaut & Mamajek 2013). For these values, and assuming a  $1.6 M_{\odot}$  neutron star (to allow for some accretion), the orbital separation is  $< 1.94 R_{\odot}$  and the Roche-lobe radius of the companion is  $< 0.56 R_{\odot}$  (Eggleton 1983), consistent with the star almost filling its Roche lobe. Alternatively, the companion may be slightly bloated compared to a main-sequence star of the same mass, as has been found in several studies of redbacks (Li et al. 2014;

Bellm et al. 2016; Linares et al. 2017).

The inclination of the orbit must be substantial in order to account for the observed optical modulation. The mass function of  $0.69 \pm 0.11 M_{\odot}$  places some limits on the inclination for reasonable values of the stellar masses. Assuming a companion mass in the range of  $0.3 < M_c < 0.5 M_{\odot}$  and a neutron star of  $1.4 < M_{\text{ns}} < 2 M_{\odot}$ , the inclination angle must be  $46^{\circ} < i \leq 90^{\circ}$ .

At minimum light,  $r' \approx 20.6$  corresponds to a distance  $< 1.7 \text{ kpc}$  for a star of type M1 or later, including the Galactic extinction in this direction of  $A_{r'} = 0.38$  (Schlafly & Finkbeiner 2011). The  $0.3\text{--}10 \text{ keV}$  X-ray luminosity of the source is  $2 \times 10^{31} (d/1 \text{ kpc})^2 \text{ erg s}^{-1}$  (Paper I), which is in the range of BWs or redbacks in the radio-pulsar state (Roberts et al. 2015). In contrast, accreting redbacks have an average  $L_x \sim 3 \times 10^{33} \text{ erg s}^{-1}$  (Bogdanov et al. 2015), with even brighter flares. The  $0.1\text{--}100 \text{ GeV}$  luminosity of 3FGL J0838.8–2829,  $1.5 \times 10^{33} (d/1 \text{ kpc})^2 \text{ erg s}^{-1}$  (Acero et al. 2015), is compatible with the pulsed emission having  $\sim 10\%$  of the spin-down power of the putative pulsar, an average efficiency observed among  $\gamma$ -ray MSPs (Abdo et al. 2013).

### 4.2. Heating Light Curve

Because its spectral type, hydrogen emission, and moderate ( $\approx 1 \text{ mag}$ ) orbital variation suggest that it has a nearly Roche-lobe filling main-sequence secondary, the optical properties of XMMU J083850.38–282756.8 are consistent with those of a redback MSP in its “radio-pulsar” (non-accreting) state. Its light curve resembles that of the brighter 4.75 hr redback PSR J1023+0038 (Woudt et al. 2004; Thorstensen & Armstrong 2005) and even more so the 6.01 hr redback PSR J1048+2339 (Deneva et al. 2016), the latter being quite similar to XMMU J083850.38–282756.8 in its apparent magnitude,  $\approx 1 \text{ mag}$  orbital modulation, and occasional bright flares. In contrast, a BW, with its substellar companion, sometimes deficient in hydrogen and usually underfilling its Roche lobe, is modulated by several magnitudes around the orbit, e.g., the 94 minute binary PSR J1311–3430 (Romani et al. 2012, 2015) and others (Breton et al. 2013; Tang et al. 2014; Romani et al. 2016).

The asymmetry of the heating light curve of XMMU J083850.38–282756.8 recalls the similar behavior of PSR J1023+0038 (Woudt et al. 2004; Bogdanov et al. 2011) in optical and X-rays, as well as PSR J1048+2339 in optical (Deneva et al. 2016). Both of these pulsars have sloping maxima, which are highest at  $\phi \approx 0.6$  and decrease toward  $\phi \approx 1.0$ . The only difference in XMMU J083850.38–282756.8 is that the slope is reversed, at least in its apparently quiescent state, increasing from  $\phi \approx 0.5$  to  $\phi \approx 0.9$  instead of decreasing. Romani & Sanchez (2016) have attempted to model such asymmetries using the effect of the orbital motion on the shape of an intrabinary shock, but the impact on the optical heating light curve is much smaller than what we observe, requiring an additional physical mechanism to explain such extreme behavior.

Romani & Sanchez (2016), as well as Tang et al. (2014) and Li et al. (2014), suggest that direct channeling of the pulsar wind by magnetic fields intrinsic to the companion star may produce asymmetric heating pat-

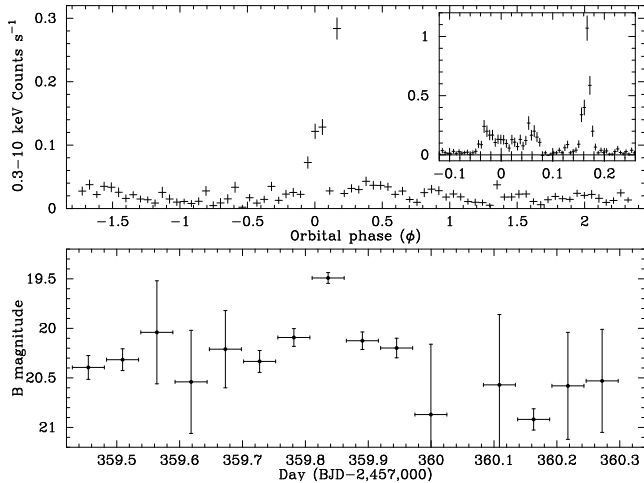


FIG. 4.— Background-subtracted *XMM-Newton* light curves, adapted from Paper I. Top: EPIC pn 0.3–10 keV light curve in 1000 s bins on 2015 December 2 (ObsID 0790180101) as a function of orbital phase extrapolated from the ephemeris in Table 2. The integer phase corresponds to the ascending node of the putative pulsar. The inset shows the 1.2 hr flaring episode at a higher resolution (100 s bins). Bottom: simultaneous *XMM-Newton* OM magnitudes from 4400 s exposures in *B*-band.

terns. Sanchez & Romani (2017) have begun to model such heating, and it appears that their offset dipole magnetic field geometry produces a light curve that resembles the data. Such strong magnetic fields can be expected in the tidally locked, rapidly rotating stars in BW and redback binaries. This also implies that large starspots could be present whose intrinsic brightness distribution could be responsible for light-curve asymmetries and variations. van Staden & Antoniadis (2016) found evidence for such spots during intensive monitoring of the redback PSR J1723–2737, which sometimes shows a periodic component slightly displaced from the orbital period, implying that the companion’s rotation is not exactly tidally locked.

#### 4.3. Optical and X-ray Flares

Definite flaring behavior is present during some of the observations, most notably during  $0.6 < \phi < 0.85$  on 2017 January 28 and February 25. In the BW PSR J1311–3430, bright flares have been seen in optical and X-rays, which, because they appear to exceed the spin-down power of the pulsar, could be coming from stored energy in the companion’s magnetic field (Romani et al. 2015). The same may be true of the occasional flares seen from PSR J1048+2339 in the Catalina Real Time Transient Survey (Deneva et al. 2016), which are difficult to account for assuming isotropic pulsar-wind heating. We do not know the pulsar parameters for XMMU J083850.38–282756.8, so it is not yet possible to make such a quantitative comparison for it.

XMMU J083850.38–282756.8 is the first non-accreting MSP binary in which a simultaneous X-ray and optical flare was observed (Paper I). The optical ephemeris of Table 2 is precise enough to extrapolate to the epoch of the *XMM-Newton* light curve of 2015 December 2 (ObsID 079018010), enabling us to examine the orbital dependence of the X-ray variability. The phase uncertainty of the extrapolation is  $\sigma(\phi) \approx 0.05$ . Figure 4 is a reproduction of Figure 10 from Paper I, now plotted as a

function of orbital phase. The dramatic 1.2 hr long flare spans  $-0.05 < \phi < 0.19$ , with peaks at  $\phi = -0.03, 0.06$ , and  $0.17$ . The flare’s final and highest peak has a maximum luminosity of  $\approx 1 \times 10^{33} (d/1 \text{ kpc})^2 \text{ erg s}^{-1}$  in a single 100 s bin. Since it occurs close to  $\phi = 0.25$ , either the flaring region must not be very close to the heated photosphere where it could be occulted, or the inclination angle of the orbit must not be very large. In redbacks there is often a broad dip in the X-ray emission centered around  $\phi = 0.25$ , which is attributed to the occultation of an intrabinary shock that is very close to the companion (Bogdanov et al. 2014a,b; Gentile et al. 2014; Hui et al. 2015; Roberts et al. 2015; Romani & Sanchez 2016). There is no evidence for such orbital modulation of the “quiescent” emission in Figure 4, which instead may be dominated by low-level flaring.

The simultaneous flare in the *XMM-Newton* optical monitor (Figure 4, bottom), for which  $B = 19.5$  averaged over the 4400 s exposure time is an increase of  $\approx 1.5$  mag over the quiescent level, is more intense than any of the smaller flares that we have seen in 33 hours of  $r'$ -band photometry. This implies either that the flares are very blue, or that emission at the level of the *XMM-Newton* flare is relatively rare.

#### 4.4. $H\alpha$ Emission

The broad width of the  $H\alpha$  emission line suggests that it is not associated with the chromosphere of the companion. Instead, it could be due to a wind driven from the heated side of the companion by the impact of the pulsar wind, or by the indirect radiation from an intrabinary shock. Alternatively, it could be associated with an accretion disk around the primary, although we disfavor this scenario because there is no other signature of a disk, e.g., a hot optical continuum. Limited by the small number of spectra collected, we see no definite pattern in velocity that could locate the origin of the line emission. However, it appears that often, but not always, there is a peak in the line profile at or near the radial velocity of the companion, which suggests that a wind is being launched from the star. Romani et al. (2015) found similar, variable He I emission lines in PSR J1311–3430, which they attributed to a wind from the companion.

It may be relevant that the strongest  $H\alpha$  emission was observed on 2017 February 12, between the January 28 and February 25 light curves when the optical continuum flaring was strongest. In contrast, on March 28 the  $H\alpha$  was weakest, while the simultaneous continuum light curve fortuitously obtained on that night showed no flaring. In any case, the large changes in equivalent width and profile suggest that a variable stellar wind is involved in producing the  $H\alpha$  emission.

## 5. CONCLUSIONS AND FURTHER WORK

A photometric and spectroscopic study of the previously suggested X-ray counterpart of the *Fermi* source 3FGL J0838.8–2829 reveals a 5.15 hr orbit with a heating light curve, and an M dwarf companion characteristic of a redback MSP system. X-ray and  $\gamma$ -ray fluxes are compatible with an MSP identification at a typical distance and spin-down power for *Fermi* MSPs. Following on similar discoveries of this distinctive class of MSP binary in positional coincidence with  $\gamma$ -ray sources, we

conclude that XMMU J083850.38–282756.8 is the redback counterpart of 3FGL J0838.8–2829 even though its pulsations have not yet been detected. This source adds to a growing sample of redbacks that have asymmetric heating light curves and strong flaring activity in X-ray and optical that are not well fitted by existing models of heating mediated by an intrabinary shock between the pulsar wind and the companion’s wind. This suggests that magnetic fields intrinsic to the companion shape the light curve, both by channeling the pulsar wind directly to its photosphere and by tapping its own energy in transient reconnection events.

Variable H $\alpha$  emission may be coming from the wind driven from the companion, which could be responsible for the absence (so far) of detected radio pulsations due to free-free absorption or dispersion. Nevertheless, sensitive searches are warranted for radio pulsations at a number of epochs and at all orbital phases, since the uncertain configuration and possibly variable column density of the absorbing plasma may allow rare windows of transparency. A search of the *Fermi*  $\gamma$ -rays for pulsations may also be feasible with the aid of the optical ephemeris, to be refined in the future.

## 6. ACKNOWLEDGEMENTS

We thank the anonymous referee for excellent suggestions. Jessica Klusmeyer obtained two of the optical light curves at the MDM Observatory. MDM Observatory is operated by Dartmouth College, Columbia University, the Ohio State University, Ohio University, and the University of Michigan. This work makes use of observations from the LCO network and the SOAR telescope, which is a joint project of the Ministério da Ciência, Tecnologia, e Inovação (MCTI) da República Federativa do Brasil, the U.S. National Optical Astronomy Observatory (NOAO), the University of North Carolina at Chapel Hill (UNC), and Michigan State University (MSU). Support for this work was provided by the National Aeronautics and Space Administration through *Chandra* Award Number SAO GO6-17027X issued by the *Chandra* X-ray Observatory Center, which is operated by the Smithsonian Astrophysical Observatory for and on behalf of the National Aeronautics Space Administration under contract NAS8-03060. J.S. acknowledges support from NASA grant NNX15AU83G and a Packard Fellowship. This investigation also uses observations obtained with *XMM-Newton*, an ESA science mission with instruments and contributions directly funded by ESA Member States and NASA.

## REFERENCES

- Abdo, A. A., Ajello, M., Allafort, A., et al. 2013, *ApJS*, 208, 17  
 Acero, F., Ackermann, M., Ajello, M., et al. 2015, *ApJS*, 218, 23  
 Ackermann, M., Ajello, M., Allafort, A., et al. 2012, *ApJ*, 753, 83  
 Alpar, M. A., Cheng, A. F., Ruderman, M. A., & Shaham, J. 1982, *Nature*, 300, 728  
 Archibald, A. M., Stairs, I. H., Ransom, S. M., et al. 2009, *Science*, 324, 1411  
 Bassa, C. G., Patruno, A., Hessels, J. W. T., et al. 2014, *MNRAS*, 441, 1825  
 Bellm, E. C., Kaplan, D. L., Breton, R. P., et al. 2016, *ApJ*, 816, 74  
 Bogdanov, S., Archibald, A. M., Hessels, J. W. T., et al. 2011, *ApJ*, 742, 97  
 Bogdanov, S., Esposito, P., Crawford, F., et al. 2014a, *ApJ*, 781, 6  
 Bogdanov, S., Patruno, A., Archibald, A. M., et al. 2014b, *ApJ*, 789, 40  
 Bogdanov, S., Archibald, A. M., Bassa, C., et al. 2015, *ApJ*, 806, 148  
 Bogdanov, S., & Halpern, J. P. 2015, *ApJL*, 803, L27  
 Breton, R. P., van Kerkwijk, M. H., Roberts, M. S., E., et al. 2013, *ApJ*, 769, 108  
 Brown, T. M., Baliber, N., Bianco, F. B., et al. 2013, *PASP*, 125, 1031  
 Camilo, F., Reynolds, J. F., Ransom, S. M., et al. 2016, *ApJ*, 820, 6  
 Clemens, J. C., Crain, J. A., Anderson, R. 2004, *Proc. SPIE*, 5492, 331  
 Deneva, J. S., Ray, P. S., Camilo, F., et al. 2016, *ApJ*, 823, 105  
 Eastman, J., Siverd, R., & Gaudi, S. B. 2010, *PASP*, 122, 935  
 Eggleton, P. P. 1983, *ApJ*, 268, 368  
 Gentile, P. A., Roberts, M. S. E., McLaughlin, M. A., et al. 2014, *ApJ*, 783, 69  
 Halpern, J. P., Bogdanov, S., & Thorstensen, J. R. 2017, *ApJ*, 838, 124 (Paper 1)  
 Hui, C. Y., Hu, C. P., Park, S. M. 2015, *ApJL*, 801, L27, *PSR J2129–0429*  
 Kataoka, J., Yatsu, Y., Kawai, N., et al. 2012, *ApJ*, 757, 176  
 Kong, A. K. H., Huang, R. H. H., Cheng, K. S., et al. 2012, *ApJL*, 747, L3  
 Kong, A. K. H., Jin, R., Yen, T.-C. 2014, *ApJ*, 749, 22  
 Lee, K. J., Guillemot, L., Yue, Y. L., Kramer, M., & Champion, D. J. 2012, *MNRAS*, 424, 2832  
 Li, M., Halpern, J. P., & Thorstensen, J. R. 2014, *ApJ*, 795, 115  
 Li, K.-L., Kong, A. K. H., Hou, X., et al. 2016, *ApJ*, 833, 143  
 Linares, M., Miles-Páez, P., Rodríguez-Gil, P., et al. 2017, *MNRAS*, 465, 4602  
 Martini, P., Stoll, R., Derwent, M. A., et al. 2011, *PASP*, 123, 187  
 Mirabal, N., Fras-Martinez, V., Hassan, T., & Fras-Martinez, E. 2012, *MNRAS*, 424, L64  
 Mirabal, N., Charles, E., Ferrara, E. C., et al. 2016, *ApJ*, 825, 69  
 Monet, D. G., Levine, S. E., Canzian, B., et al. 2003, *AJ*, 125, 984  
 Papitto, A., Ferrigno, C., Bozzo, E., et al. 2013, *Nature*, 501, 517  
 Pecaut, M. J. & Mamajek, E. E. 2013, *ApJS*, 208, 9  
 Pletsch, H. J., Guillemot, L., Fehrmann, H., et al. 2012, *Science*, 338, 1314  
 Ray, P. S., Belfiore, A. M., Saz Parkinson, P., et al. 2014, *BAAS*, 223, #140.07  
 Rea, N., Coti Zelati, F., Esposito, P., et al. 2017, *MNRAS*, in press (arXiv:1611.04194)  
 Roberts, M. S. E. 2013, in *Proc. IAU Symp.* 291, *Neutron Stars and Pulsars: Challenges and Opportunities after 80 years*, ed. J. van Leeuwen (Cambridge: Cambridge Univ. Press), 127  
 Roberts, M. S. E., McLaughlin, M. A., Gentile, P. A., et al. 2015, in *Fifth Int. Fermi Symp. Proc.* arXiv:1502.07208  
 Romani, R. W., & Shaw, M. S. 2011, *ApJL*, 743, 26  
 Romani, R. W. 2012, *ApJL*, 754, L25  
 Romani, R. W., Filippenko A. V., Silverman, J. M., et al. 2012, *ApJL*, 760, L36  
 Romani R. W., Filippenko A. V., & Cenko S. B. 2014, *ApJL*, 793, L20  
 Romani, R. W. 2015, *ApJL*, 812, L24  
 Romani, R. W., Filippenko, A. V., & Cenko S. B. 2015, *ApJ*, 804, 115  
 Romani, R. W., Graham, M. L., Filippenko, A. V., & Zheng, W. 2016, *ApJ*, 833, 138  
 Romani, R. W., & Sanchez, N. 2016, *ApJ*, 828, 7  
 Roy, J., Ray, P. S., Bhattacharyya, B., et al. 2015, *ApJL*, 800, L12  
 Salvetti, D., Mignani, R. P., De Luca, A., et al. 2015, *ApJ*, 814, 888  
 Sanchez, N., & Romani, R. W. 2017, *ApJ*, in press (arXiv:1706.05467)  
 Saz Parkinson, P. M., Xu, H., Yu, P. L. H., et al. 2016, *ApJ*, 820, 8  
 Schlafly, E. F., & Finkbeiner, D. P. 2011, *ApJ*, 737, 103  
 Strader, J., Chomiuk, L., Sonbas, E., et al. 2014, *ApJL*, 788, L27  
 Strader, J., Chomiuk, L., Cheung, C. C., et al. 2105, *ApJL*, 804, L12  
 Strader, J., Li, K.-L., Chomiuk, L., et al. 2016, *ApJ*, 831, 89  
 Tang, S., Kaplan, D. L., Phinney, E. S., et al. 2014, *ApJL*, 791, 5  
 Tavani, M. 1991, *ApJ*, 379, L69  
 Thorstensen, J. R., & Armstrong, E. 2005, *ApJ*, 130, 759  
 van Staden, A. D., & Antoniadis, J. 2016, *ApJL*, 833, L12  
 Woudt, P. A., Warner, B., & Pretorius, M. L. 2004, *MNRAS*, 351, 1015